Supplementary Materials for

Dynamic and multivalent engagement determines context-dependent nucleosomal deacetylation by the Rpd3S complex

Haipeng Guan[#], Pei Wang[#], Pei Zhang, Chun Ruan, Yutian Ou, Bo Peng, Xiangdong Zheng, Jianlin Lei, Bing Li, Chuangye Yan* and Haitao Li*

[#] These authors contributed equally to this work.

* Correspondence: yancy2019@tsinghua.edu.cn; lht@tsinghua.edu.cn

Materials and Methods

Protein Expression and Purification

The components of the Rpd3S complex, including full-length Rpd3, Sin3, Rco1, Ume1, and Eaf3, were amplified from total yeast DNA by PCR. All of these components and their mutants were cloned into modified pFastbac baculoviral expression vectors. A TEV-cleavable Strep-tag was engineered at the N-terminus of Rco1 for affinity purification. The bac-to-bac baculovirus system was used to express the target protein in insect cells. Baculovirus of all components of Rpd3S were mixed in a predetermined ratio to achieve stoichiometric expression in cells. Sf9 insect cells were co-transfected at 27℃ for 72 h. Cells were harvested by centrifugation at 4℃, 2700 rpm for 20 min, and the pellet was resuspended by cell lysis buffer (20 mM Tris-HCl pH 7.5, 300 mM NaCl, 5% glycerol, 0.1% NP-40) supplied with 1 mM PMSF and a protease inhibitor cocktail. Cells in the lysis buffer were sonicated using 56% amplification with 3s on and 7s pulse for 15min on ice. Cell debris were removed by centrifugation at 4℃, 25,000 rpm for 1 h. The cleared lysate was co-incubated with strep beads and then successively washed by cell lysis buffer, and the target protein was finally eluted by elution buffer (100 mM Tris-HCl pH 8.0, 150 mM NaCl, 10mM D-desthiobiotin). Fractions containing Rpd3S were incubated overnight at 4 °C with TEV protease to cleave off the tag. The digested protein was further purified by an Anion exchange column (GE® healthcare). Target proteins were collected, concentrated and purified by size-exclusion chromatography

using a Superose 6 Increase 5/150 GL column (GE® healthcare) in buffer (20 mM HEPES pH 7.5, 150mM NaCl).

Nucleosome reconstitution

Widom 601 sequence and a 20-bp linker DNA emitting from one side were purified from a plasmid encoding 20 repeats (each flanked by the EcoRV restriction enzyme cutting site) of the sequence as previously described[41]. The full-length unmodified *Xenopus laevis* histones H2A, H2B, H3, and H4 were expressed in *Escherichia coli* strain BL21 (DE3) and purified using a previously reported method[42]. All modified H3 or H4 were synthesized by KS-V Peptide (KS-V Peptide Co., Hefei, China). Histone octamers containing either unmodified, K36me3 H3, or acetylated H3/H4 were refolded as previously described[41]. A modification of the salt gradient method described by Thomas and Butlerz[43] was used for the reconstitution of histone octamer with DNA. Histone octamer and DNA were combined at 2 M NaCl; the gradual reduction of the salt concentration to 0.25 M NaCl over a period of 36 h led to the formation of NCPs.

Sample preparation and cryo-EM data collection

The Rpd3S–NCP complex was obtained by mixing 15μM protein with 5μM NCP. We purified and stabilized the Rpd3S and Rpd3S–NCP complexes using the GraFix method[44]. To form the gradient, a 6 mL top solution containing 50 mM NaCl, 20 mM HEPES (pH 7.5), and 10% glycerol (Sigma) was added to a tube (Beckman, 331372). The bottom solution (6 mL) containing 50 mM NaCl, 20 mM HEPES (pH 7.5), 30% glycerol, and 0.15% glutaraldehyde was then injected into the bottom of the tube using a syringe with a blunt-ended needle. The tubes were placed into a gradient master (BioComp) to form a continuous density and glutaraldehyde gradient. Finally, 200 μL of sample was loaded. The sample tubes were ultracentrifuged at 4°C for 14 h at a speed of 35,000 rpm. (Beckman, Rotor SW-41Ti). Fractions were collected every 500 μL. The best fractions were selected and dialyzed to buffer (20 mM HEPES pH 7.5, 50mM NaCl, 3% glycerol) for EM sample preparation. For cryo-EM, an aliquot of 4 μL of the sample at a concentration of ~0.2 mg/mL was applied to glow-discharged grids (Quantifoil 1.2/1.3). The grids were then blotted for 3.5 s and plunged into liquid ethane cooled by liquid nitrogen, using a Vitrobot (FEI). The EM grids were imaged on

a Titan Krios transmission electron microscope (FEI) operated at 300 kV. A total of 6,990 images of the Rpd3S complex were collected on K3 (Gatan) with a pixel size of 0.55 Å/pixel, and a total of 10,786 images of Rpd3S-nucleosome were collected on K3 (Gatan) with a pixel size of 0.541 Å/pixel. AutoEMation2 was used for automated data collection[45]. Defocus was set automatically, with values ranging from -1.5 to -1.8 μm. The fluence was ~50e^-/ Å2 fractionated into 32 frames (exposure time 2.56s).

Image processing

Motion correction was performed using the MotionCor2[46]. CTF parameters were estimated using GCTF[47]. For the Rpd3S complex dataset, after automatic particle picking and 3 rounds of 2D classification in RELION[48,49], ~2.63M particles were selected for the first round of 3D classification. The initial model was generated by RELION and low-pass-filtered to 60 Å for a 3D reference. After 2 rounds of 3D classification, ~670k particles were selected and used for 3D auto-refinement and post-processing, resulting in a reconstruction of the entire Rpd3S complex at 3.2Å. Following local mask 3D classification for head-bridge-right arm, ~348k particles were selected and 3D auto-refined and post-processed, resulting in a local density map of the head-bridge-right arm with a resolution of 2.7 Å. Similarly, the local density map of the bridge-left arm was reconstructed at 3.2 Å. For the Rpd3S-nucleosome complex datasets, two datasets of 10,786 micrographs were selected. After automatic particle picking and 2 rounds of 2D classification in RELION, ~2.59M particles were selected for 3D classification. The initial model was generated by RELION and low-pass-filtered to 60 Å for a 3D reference. After 2 rounds of 3D classification, two representative classes of the Rpd3S-nucleosome complex were relatively better distinguished with the change of the Rpd3S complex on the nucleosome. For the CHD-nucleosome, ~427k particles were used to 3D auto-refine and post-process in a close state, resulting in a local density map of the CHD-nucleosome with a resolution of 2.8 Å. After one round of 3D classification on the Rpd3S complex, two classes were performed respectively, resulting in two distinguished states of the stable Rpd3S complexes. All two classes were subject to global 3D refinement, yielding two density maps at resolutions of 4.0 Å (close state), 4.0 Å (loose state). After 3D refinement of Rpd3S complex, a 3.3 Å map and a 3.4 Å map of the Rpd3S in two classes were resolved, respectively.

The local resolution map was created using RELION[49] and represented using UCSF Chimera[50]. All reported resolutions are based on the gold-standard Fourier shell correlation (FSC) 0.143. The final FSC curves were corrected for the effect of a soft mask with high-resolution noise substitution.

Model building

The whole structural model of the Rpd3S complex was manually built in COOT[51] according to the 2.7-Å map of the head-bridge-right arm region and a 3.2 Å map of the bridge-left arm region. AlphaFold was used to predict and determine the special knotted coil in Rco1[52]. The structures of the nucleosome (PDB ID: 6ESF) and Eaf3-CHD (PDB ID: 3E9G) served as initial structural templates for the CHD-nucleosome model, which was docked into the cryo-EM maps using UCSF Chimera[50]. The $CHD_{Eaf3\text{-}A}$ was built and adjusted in COOT, while $CHD_{Eaf3\text{-}B}$ was docked into the cryo-EM map. Two structural models of the Rpd3S-nucleosome were built by docking the Rpd3S complex and CHD-nucleosome structures into a 2.8 Å map of CHD-nucleosome, a 3.3 Å map, and a 3.4 Å map of the Rpd3S complex respectively in two states, followed by rigid-body fitting and manual model building. The models were refined in real space using Phenix[53]. Statistics of the map reconstruction and model refinement were shown in Supplementary Table 1 and 2. The final models were evaluated using MolProbity[54]. Map and model representations in the figures were prepared by PyMOL (https://pymol.org/), UCSF Chimera[50] or UCSF ChimeraX[55].

Isothermal titration calorimetry

All calorimetric experiments on the wild-type or mutant PHD1 domain of Rco1 proteins were conducted at 25 °C using a MicroCal PEAQ-ITC instrument (Malvern Panalytical). All proteins and synthetic histone peptides were prepared under the same titration buffer containing 20 mM Tris 7.5, 50 mM NaCl, and 5% glycerol. The protein concentration was determined by absorbance spectroscopy at 280 nm. Peptides (>95% purity) were quantified by weighing on a large scale, aliquoted, and freeze-dried for individual use. Acquired calorimetric titration curves were analyzed using Origin 7.0 (OriginLab) with the “One Set of Binding Sites” fitting model. The detailed peptide sequence information is $H3_{1–10}$un: ARTKQTARKS.

HDAC assays

For the Rpd3S deacetylation assays, the H3/H4Kac and H3K36me3 nucleosomes (500nM) assembled *in vitro* were treated with different Rpd3S complexes at different concentrations in a buffer with 20 mM HEPES 7.5, 150mM NaCl, and 0.2 mg/mL BSA at 30°C. For the differences in enzyme activity caused by different histone modifications and H3K9R mutant, we adopted the enzyme activity assays in a buffer with 20 mM HEPES 7.5, 150mM NaCl, 0.2 mg/mL BSA and 0.15μg/μL salmon sperm DNA at 30°C. For nucleosome samples, 80 mM EDTA and 5x SDS-PAGE gel loading buffer were added after 25 minutes. The samples were boiled for 5 min at 95°C and resolved by 4-20% SDS-PAGE. After transferring to PVDF membrane, H3K9ac, H3K14ac, H3K18ac, H3K23ac, H3K27ac, H4K5ac, H4K8ac, H4K12ac, H4K16ac, and total H4 were detected by western blot with specific antibodies on separate gels. Western blot bands were visualized by ECL.

Cross-linking Mass Spectrometry

The purified Rpd3S complex was cross-linked with 5 mM bis (sulfosuccinimidyl) suberate (BS3) at room temperature for 2h. The reaction was quenched with 40 mM Tris-HCl pH 7.5. The cross-linked sample was then excised for in-gel digestion and identified by mass spectrometry. To begin the in-gel digestion process, the sample was disulfide-reduced with 25 mM dithiothreitol (DTT) and alkylated with 55 mM iodoacetamide. In-gel digestion was performed using sequencing grade-modified trypsin in 50 mM ammonium bicarbonate at 37 °C overnight. The peptides were extracted twice with 1% trifluoroacetic acid in a 50% acetonitrile aqueous solution for 30 min. The peptide extracts were then centrifuged in a SpeedVac to reduce the volume.

For LC-MS/MS analysis, peptides were separated by a 60 min gradient elution at a flow rate 0.300 μL/min with a Thermo-Dionex Ultimate 3000 HPLC system, which was directly interfaced with the Thermo Orbitrap Fusion mass spectrometer. The analytical column was a homemade fused silica capillary column (75 μm ID, 150 mm length; Upchurch, Oak Harbor, WA) packed with C-18 resin (300 A, 5 μm; Varian, Lexington, MA). Mobile phase A consisted of 0.1% formic acid, and mobile phase B consisted of 100% acetonitrile and 0.1% formic acid. The Orbitrap Fusion mass spectrometer was operated in the the data-dependent acquisition

mode using Xcalibur3.0 software, and there was a single full-scan mass spectrum in the Orbitrap (350-1550 m/z, 120,000 resolution) followed by 3 seconds data-dependent MS/MS scans in an Ion Routing Multipole at 30% normalized collision energy (HCD). The MS/MS spectra from each LC-MS/MS run were searched against the selected database using Proteome Discovery searching algorithm (version 1.4). Raw data were processed with pLink2 software[56]. A crosslink network diagram was prepared using xiNET[57].

Computational docking of $H3_{1-16}$K14ac into Rpd3S complex

The readouts of histone H3K4un by the PHD1 of Rco1 and PHD of BHC80 are highly conserved. Additionally, Rpd3 is highly conserved with HDAC1. Based on this information, structures of the Rpd3S and Rpd3S-H3K36me3 nucleosome complexes, BHC80-PHD (PDB ID: 2PUY), and HDAC1-H4K16Hx (PDB ID: 5ICN) were prepared for docking using the protein-preparation wizard in Maestro (Schrödinger Release 2018-1: Maestro, Schrödinger). Hydrogens were added and the protonation states of titratable amino acids were determined during the protein-preparation. Docking was then performed using GLIDE/SP-peptide in Schrödinger[58]. Histone $H3_{1-7}$K4un was docked into the PHD1 of Rco1-A and histone $H3_{12-16}$K14ac was docked into the HDAC catalytic pocket of Rpd3. Simultaneously, $H3_{8-11}$ was stretched out between $H3_{1-7}$K4un and $H3_{12-16}$K14ac, hindered by hydrogen bond interactions and steric hindrance.

Spotting assays

The Rco1 and mutants, along with their native promoters, were cloned onto pRS415 plasmids. The plasmids (including control plasmid) were then transformed into the *STE11-HIS3* reporter strain (YBL853). To analyze the growth of the yeast strains, 5-fold serially dilutions of fresh culture concentrated to an OD600 of 0.4 were spotted onto the SC-Leu (control) and SC-His-Leu plates until saturation.

To analyze the importance of H3K9ac on yeast growth, we used a CRISPR–Cas9 genome editing method[59] to target the *HTT1* and *HTT2* genes and obtain the H3K9R mutant in the W303-1a strain. The cells were diluted to an OD of 0.4 and 5-fold serially diluted. About 5 μL of each dilution was spotted on a 100 μg/mL 6-AU plate until saturation.

Western blotting

To examine the levels of acetylation caused by Rco1 mutants *in vivo*, the Rco1 wild type and mutants, along with their native promoters, were cloned to pRS415 plasmids. The plasmids were then transformed into an Rco1 deleted strain (YBL534). The yeast strains were grown overnight at 30 ℃ in Leu medium, diluted to an OD600 of 0.1, and grown for another 8 h to an OD600 of 0.8-1.0. To examine the changes of H3 and H4 acetylation in an H3K9R mutant strain, the W303-1a and W303-1a-H3K9R were grown overnight at 30℃ in YPD, diluted to an OD600 of 0.1, and grown for another 8 h to an OD600 of 0.8-1.0. The protein of yeast cells was extracted as described[60]. The samples were boiled for 20 min at 95°C and resolved by 4-20% SDS-PAGE. After transferring to a PVDF membrane, H3K9ac, H3K14ac, H3K18ac, H3K23ac, H3K27ac, H3K56ac, H4K5ac, H4K8ac, H4K12ac, H4K16ac, and total H4 were detected by western blot with specific antibodies on separate gels. Western blot bands were visualized by ECL.

To examine the levels of H3K56ac caused by Rpd3S complex *in vivo*, the pRS415-Rco1 and control plasmid were then transformed into the YBL534 strain. The yeast strains were grown overnight at 30 ℃ in Leu medium, diluted to an OD600 of 0.1, and grown for another 8 h to an OD600 of 0.8-1.0. H3K9ac, H3K14ac, H3K18ac, H3K23ac, H3K27ac, H3K56ac, and total H3 were detected by western blot with specific antibodies on separate gels. Western blot bands were visualized by ECL.

All yeast strains were constructed using standard procedures and are listed in Supplemental Table 3.

Supplementary references

41 Dyer, P. N. *et al.* Reconstitution of nucleosome core particles from recombinant histones and DNA. *Method Enzymol* **375**, 23-44 (2004).

42 Luger, K., Rechsteiner, T. J. & Richmond, T. J. Preparation of nucleosome core particle from recombinant histones. *Chromatin* **304**, 3-19 (1999).

43 Richmond, T. J., Searles, M. A. & Simpson, R. T. Crystals of a Nucleosome Core Particle Containing Defined Sequence DNA. *Journal of Molecular Biology* **199**, 161-170, doi:Doi 10.1016/0022-2836(88)90386-5 (1988).

44 Stark, H. Grafix: Stabilization of Fragile Macromolecular Complexes for Single Particle Cryo-Em.

Methods in Enzymology, Vol 481: Cryo-Em, Part a - Sample Preparation and Data Collection **481**, 109-126, doi:10.1016/S0076-6879(10)81005-5 (2010).

45 Lei, J. L. & Frank, J. Automated acquisition of cryo-electron micrographs for single particle reconstruction on an FEI Tecnai electron microscope. *J Struct Biol* **150**, 69-80, doi:10.1016/j.jsb.2005.01.002 (2005).

46 Zheng, S. Q. *et al.* MotionCor2: anisotropic correction of beam-induced motion for improved cryo-electron microscopy. *Nat Methods* **14**, 331-332, doi:10.1038/nmeth.4193 (2017).

47 Zhang, K. Gctf: Real-time CTF determination and correction. *J Struct Biol* **193**, 1-12, doi:10.1016/j.jsb.2015.11.003 (2016).

48 Scheres, S. H. W. RELION: Implementation of a Bayesian approach to cryo-EM structure determination. *J Struct Biol* **180**, 519-530, doi:10.1016/j.jsb.2012.09.006 (2012).

49 Kimanius, D., Forsberg, B. & Lindahl, E. Accelerated Cryo-EM Structure Determination with Parallelisation using GPUs in Relion-2. *Biophys J* **112**, 575a-575a, doi:DOI 10.1016/j.bpj.2016.11.3096 (2017).

50 Pettersen, E. F. *et al.* UCSF chimera - A visualization system for exploratory research and analysis. *J Comput Chem* **25**, 1605-1612 (2004).

51 Emsley, P. & Cowtan, K. Coot: model-building tools for molecular graphics. *Acta Crystallogr D* **60**, 2126-2132, doi:10.1107/S0907444904019158 (2004).

52 Jumper, J. *et al.* Highly accurate protein structure prediction with AlphaFold. *Nature* **596**, 583-589, doi:10.1038/s41586-021-03819-2 (2021).

53 Adams, P. D. *et al.* PHENIX: building new software for automated crystallographic structure determination. *Acta Crystallogr D* **58**, 1948-1954, doi:10.1107/S0907444902016657 (2002).

54 Chen, V. B. *et al.* MolProbity: all-atom structure validation for macromolecular crystallography. *Acta Crystallogr D* **66**, 12-21, doi:10.1107/S0907444909042073 (2010).

55 Goddard, T. D. *et al.* UCSF ChimeraX: Meeting modern challenges in visualization and analysis. *Protein Sci* **27**, 14-25, doi:10.1002/pro.3235 (2018).

56 Yang, B. *et al.* Identification of cross-linked peptides from complex samples. *Nat Methods* **9**, 904-906, doi:10.1038/nmeth.2099 (2012).

57 Combe, C. W., Fischer, L. & Rappsilber, J. xiNET: cross-link network maps with residue resolution. *Mol Cell Proteomics* **14**, 1137-1147, doi:10.1074/mcp.O114.042259 (2015).

58 Halgren, T. A. *et al.* Glide: a new approach for rapid, accurate docking and scoring. 2. Enrichment factors in database screening. *J Med Chem* **47**, 1750-1759, doi:10.1021/jm030644s (2004).

59 Laughery, M. F. *et al.* New vectors for simple and streamlined CRISPR-Cas9 genome editing in Saccharomyces cerevisiae. *Yeast* **32**, 711-720, doi:10.1002/yea.3098 (2015).

60 Kushnirov, V. V. Rapid and reliable protein extraction from yeast. *Yeast* **16**, 857-860, doi:10.1002/1097-0061(20000630)16:9<857::AID-YEA561>3.0.CO;2-B (2000).

61 Lan, F. *et al.* Recognition of unmethylated histone H3 lysine 4 links BHC80 to LSD1-mediated gene repression. *Nature* **448**, 718-U714, doi:10.1038/nature06034 (2007).

62 Turnbull, R. E. *et al.* The MiDAC histone deacetylase complex is essential for embryonic development and has a unique multivalent structure. *Nat Commun* **11**, doi:10.1038/s41467-020-17078-8 (2020).

63 Millard, C. J. *et al.* Class I HDACs Share a Common Mechanism of Regulation by Inositol Phosphates. *Mol Cell* **51**, 57-67, doi:10.1016/j.molcel.2013.05.020 (2013).

Extended Data Figure Legends

Extended Data Figure 1. Protein purification and XL-MS analysis of Rpd3S complex. a-c. Purification of Rpd3S and mutant complexes. Purification of the Rpd3S and mutant complexes. The complexes were purified using size-exclusion chromatography (Superose 6), and the peak fractions were subjected to SDS-PAGE for Coomassie blue staining. The complexes include: (**a**) wild-type of Rpd3S complex; (**b**) Rco1-E260A/D261A of the Rpd3S complex to disrupt the PHD1 of Rco1; (**c**) Rco1-7mutants of Rpd3S complex to disrupt the left arm region. **d.** Schematic representation of the intermolecular cross-links within the Rpd3S complex. The domains of Rpd3S are indicated, and the identified inter-subunit cross-links or subunit self-links are shown as cyan or modena solid lines, respectively. The special intermolecular self-links in the C-terminal of Rco1 are shown as red solid lines.

Extended Data Figure 2. Data collection and image processing of the Rpd3S complex. Representative cryo-EM micrograph (**a**) and 2D class averages (**b**) of various projection views of the Rpd3S complex. (**c**) Flowchart of the cryo-EM image processing, 3D reconstructions for the Rpd3S complex, angular distribution, and resolution estimation of the EM maps.

Extended Data Figure 3. Cryo-EM reconstructions and structural model of the Rpd3S complex. a. Estimated resolution of the cryo-EM reconstructions of the whole Rpd3S complex. Local resolution estimation of the cryo-EM reconstructions of the head-bridge-right arm region (**b**) and the bridge-left arm region (**c**) of the Rpd3S complex. **d.** The locally refined cryo-EM map of the Rpd3S complex. Close-up views of fragments of Rpd3S subunits with cryo-EM densities shown as meshes. The residues are shown as sticks representations.

Extended Data Figure 4. Detailed structure of Rco1-SBD. a. Stereo view of the SBD domain of Rco1-A shown in cartoon form. Detailed structures of visible SBD domain of Rco1-A (**b**) and Rco1-B (**c**). Residues are depicted as sticks. **d.** Stereo view of the SBD domain of Rco1-A predicted by AlphaFold.

Extended Data Figure 5. Structural comparison of the PHD domains in Rco1. a and **b.** Comparison of the PHD1 and PHD2 of Rco1 with BHC80-PHD (PDB ID: 2PUY)[61]. **c** and **d.** Sequence conservation analysis of PHD1 and PHD2 of Rco1 with BHC80-PHD.

Extended Data Figure 6. The interface details between the core enzyme Rpd3 and its neighboring subunits. a. A global view of the interactions around the core enzyme Rpd3. The positions of interaction are marked with numbers. Detailed views of the interactions between Rpd3 and HID-N of Sin3, PHD1 of Rco1-A, Eaf3-A (**b**); LoopS of Sin3 (**c**); FHF of Sin3 (**d**); HID-C of Sin3 (**e**); αβC of Rco1-A (**f**); PHD2 of Rco1-A (**g**). Residues at the interface are depicted as sticks.

Extended Data Figure 7. Structural comparison of PAH domains. a. PAH1-SAP25 (PDB ID: 2RMS)[25], **b.** PAH2-Mad1 (PDB ID: 1G1E)[26], **c.** PAH3-Rco1 in Rpd3S complex, **d.** "PAH4" of Sin3 in the Rpd3S complex. The PAH domains are colored in green.

Extended Data Figure 8. Structural comparison of regulatory modes of HDAC complexes. a. Close-up view of interactions between the HID domain of Sin3 shown in cartoon and Rpd3 shown in surface representation. **b.** Comparison of the overall structure and key amino acids in the basic pocket of HDACs. Rpd3S is colored in blue, HDAC1 is colored in green, and HDAC3 is colored in purple. **c.** Structural comparison of HDAC complexes in inositol phosphates regulation. Rpd3S complex: Rpd3-Sin3, MiDAC complex: HDAC1-MIDEAS (PDB ID: 6Z2J)[62], SMRT complex: HDAC3-SMRT (PDB ID: 4A69)[29], NuRD complex: HDAC1-MTA1 (PDB ID: 4BKX)[63]. **d.** Sequence conservation analysis of the α2 of Sin3 from yeast to human.

Extended Data Figure 9. Data collection and image processing of Rpd3S-nucleosome. Representative cryo-EM micrograph (**a**) and 2D class averages (**b**) of various projection views of Rpd3S-nucleosome. **c.** Flowcharts of the cryo-EM image processing, angular distribution, and 3D reconstructions for the Rpd3S-nucleosome.

Extended Data Figure 10. Cryo-EM reconstructions of Rpd3S-nucleosome. Local estimated resolution of the cryo-EM reconstructions of the CHD-nucleosome (**a**), Rpd3S in close state (**b**), and Rpd3S in loose state (**c**). **d.** Resolution estimation of the EM maps in **a-c**.

Extended Data Figure 11. Cryo-EM structure of Rpd3S complex bound to H3K36me3 Nucleosome in the loose state. a. Core Rpd3S complex bound to the H3K36me3 modified nucleosome in the loose state. **b.** Stereo view of contact between core Rpd3S complex and H3K36me3 modified nucleosome in the loose state. Sin3, Rpd3, Eaf3, and Rco1 are shown in

cartoon form. Nucleosome is shown in surface representation. The invisible left arm region is colored white.

Extended Data Figure 12. The interface details between CHD domains and histone H3K36me3. a. Detailed view of interactions between CHD and H3 tail. Close-up views of the loop of CHD and H3 tail for interactions with cryo-EM densities shown as meshes. **b.** Detailed view of the interactions between Eaf3^{A}-CHD and the H3K36me3 modified nucleosome. **c.** Detailed view of the interactions between Eaf3^{B}-CHD and the H3K36me3 modified nucleosome. The residues of CHDs and H3 tail residues are shown as sticks. The positions of nucleosomal DNA are labeled with SHL numbers.

Extended Data Figure 13. The site-specificity of antibodies used in HDAC assay. a and **b.** Validation of the site-specificity of antibodies used in HDAC assay.

Extended Data Figure 14. The catalytic activity of Rpd3S on H3K4me3K36me3 nucleosome. A representative HDAC assay measuring activity of Rpd3S complex on H3K4me3K36me3 nucleosome. The reaction products were identified using Western blot.

Extended Data Figure 15. H3K36me3 promotes the catalytic activity of Rpd3S on nucleosome substrates. A representative HDAC assay measuring the activity of Rpd3S complex containing wild-type (**a**), mutants of PHD1 (**b**), and left arm region (**c**) on H3K36me3 and H3K36me0 nucleosomes. The reaction products were identified using Western blot.

Extended Data Figure 16. The catalytic activity of Rpd3S on H3K9RK36me3 nucleosome. A representative HDAC assay measuring activity of Rpd3S complex on H3K9RK36me3 nucleosome. The reaction products were identified using Western blot.

Extended Data Figure 17. The HDAC catalytic activity of Rpd3S complex distinctively on H3K9ac. A representative HDAC assay measuring the activity of Rpd3S complex in sufficient time, where only H3K9ac can be retained over time.

Extended Data Figure 18. A "seeding mark" model of "Rpd3S-NuA3/NuA4" enzymatic pairs in balancing chromatin acetylation levels during transcription. The complexes are shown in a cartoon model. The Rpd3S complex recognizes H3K36me3 and removes most N-

terminal acetylation marks of H3 and H4, except for H3K9ac. The Rpd3S-resistent H3K9ac, along with H3K36me3, may serve as "seeding marks" that can recruit NuA3 and NuA4 for the reestablishment of hyperacetylated histones H3 and H4, respectively.

Extended Data Figure 19. The H3K56ac modification is not directly affected by the Rpd3S complex *in vivo*. Western blot shows H3 acetylation levels at different sites in Rpd3S wild-type and Rco1-deleted strains. The alterations observed in H3K9ac and H3K56ac are not significant in comparison to other H3 sites in Rco1-deleted strains.

Extended Data Figure 20. The catalytic models of Rpd3S with di-nucleosome. a. The two CHD domains of Eaf3-A and Eaf3-B with PHD1 of Rco1-A are involved in recognizing one nucleosome, and PHD1 of Rco1-B is involved in recognizing another nucleosome. **b** and **c.** Two Rpd3S can bind to two nucleosomes, respectively, at a suitable 40bp linker DNA length. The latter Rpd3S complexes may be assembled on two nucleosome discs respectively.

Supplementary Table 1. Cryo-EM data collection, refinement, and validation statistics of Rpd3S complex.

Supplementary Table 2. Cryo-EM data collection, refinement, and validation statistics of Rpd3S-nucleosome.

Supplementary Table 3. Yeast Strains used in this study.

Supplementary Video 1. Cryo-EM map and model of Rpd3S complex.

Supplementary Video 2. Cryo-EM map and model of CHD-nucleosome.

Supplementary Video 3. Cryo-EM map and model of Rpd3S-nucleosome in close state.

Supplementary Video 4. Cryo-EM map and model of Rpd3S-nucleosome in loose state.

Supplementary Video 5. The dynamic change of Rpd3S complex on nucleosome in H4 deacetylation.

Supplementary Data 1. XL-MS analysis of Rpd3S complex.

Extended Data Figure 1

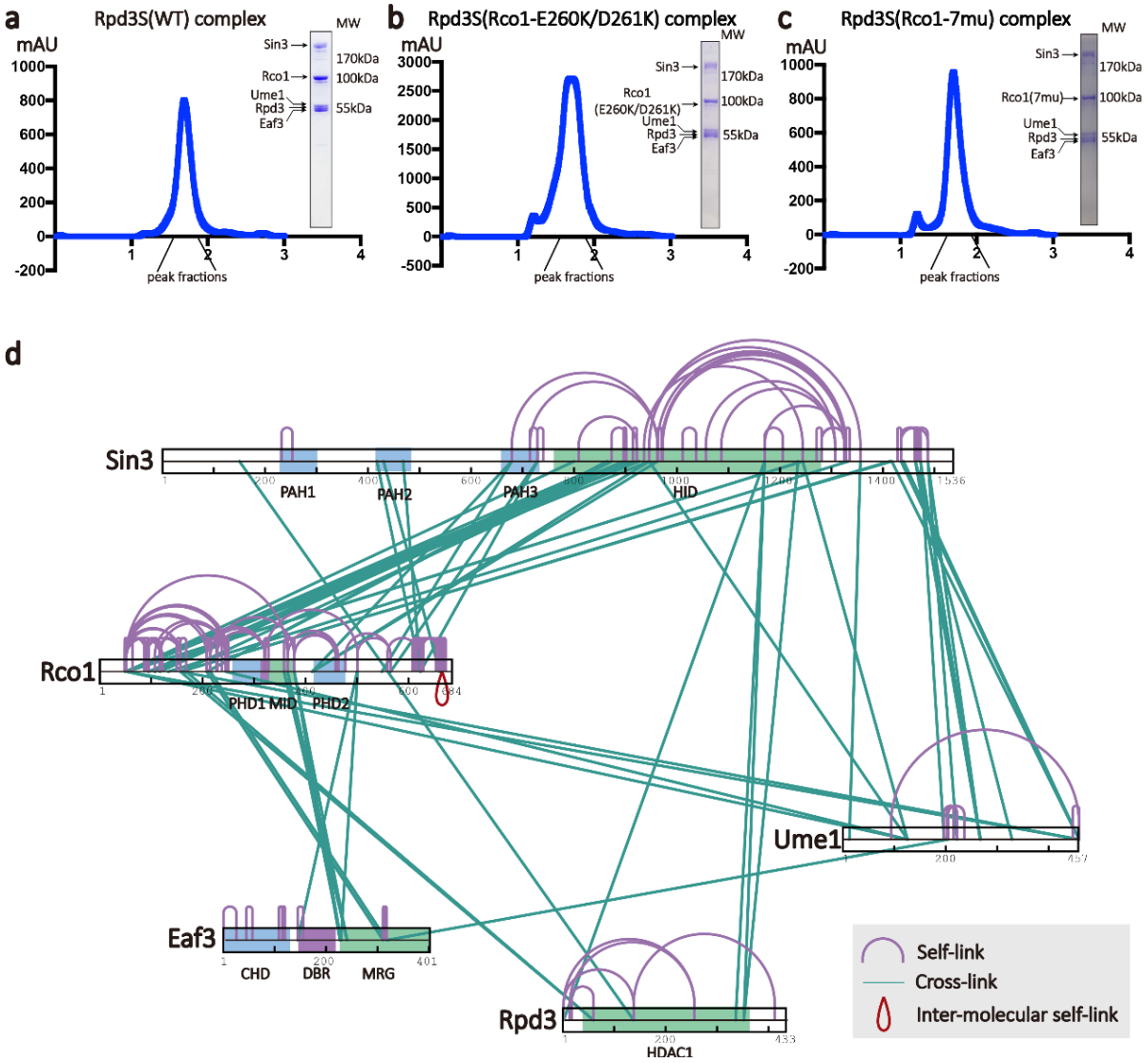

Extended Data Figure 2

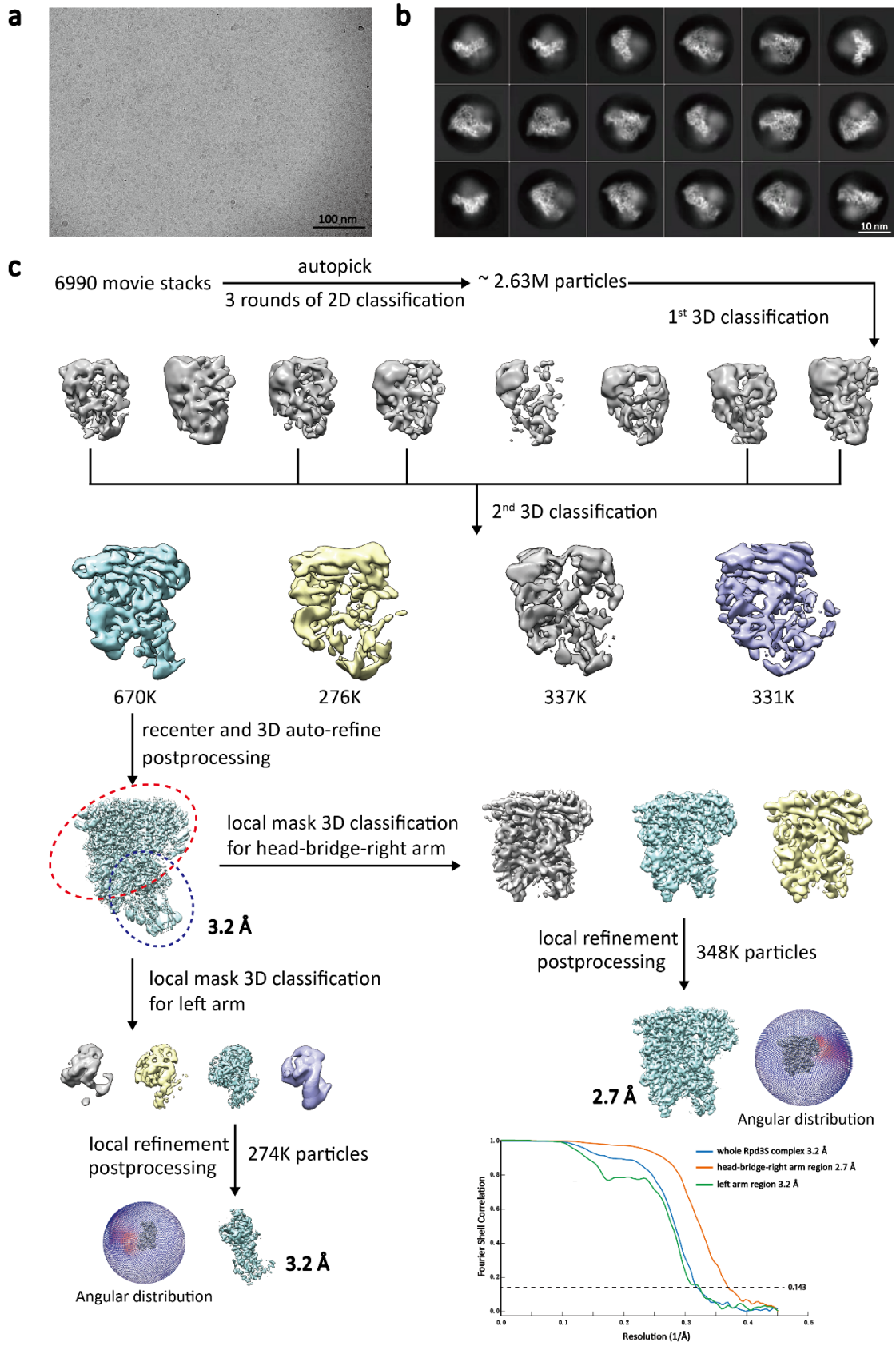

Extended Data Figure 3

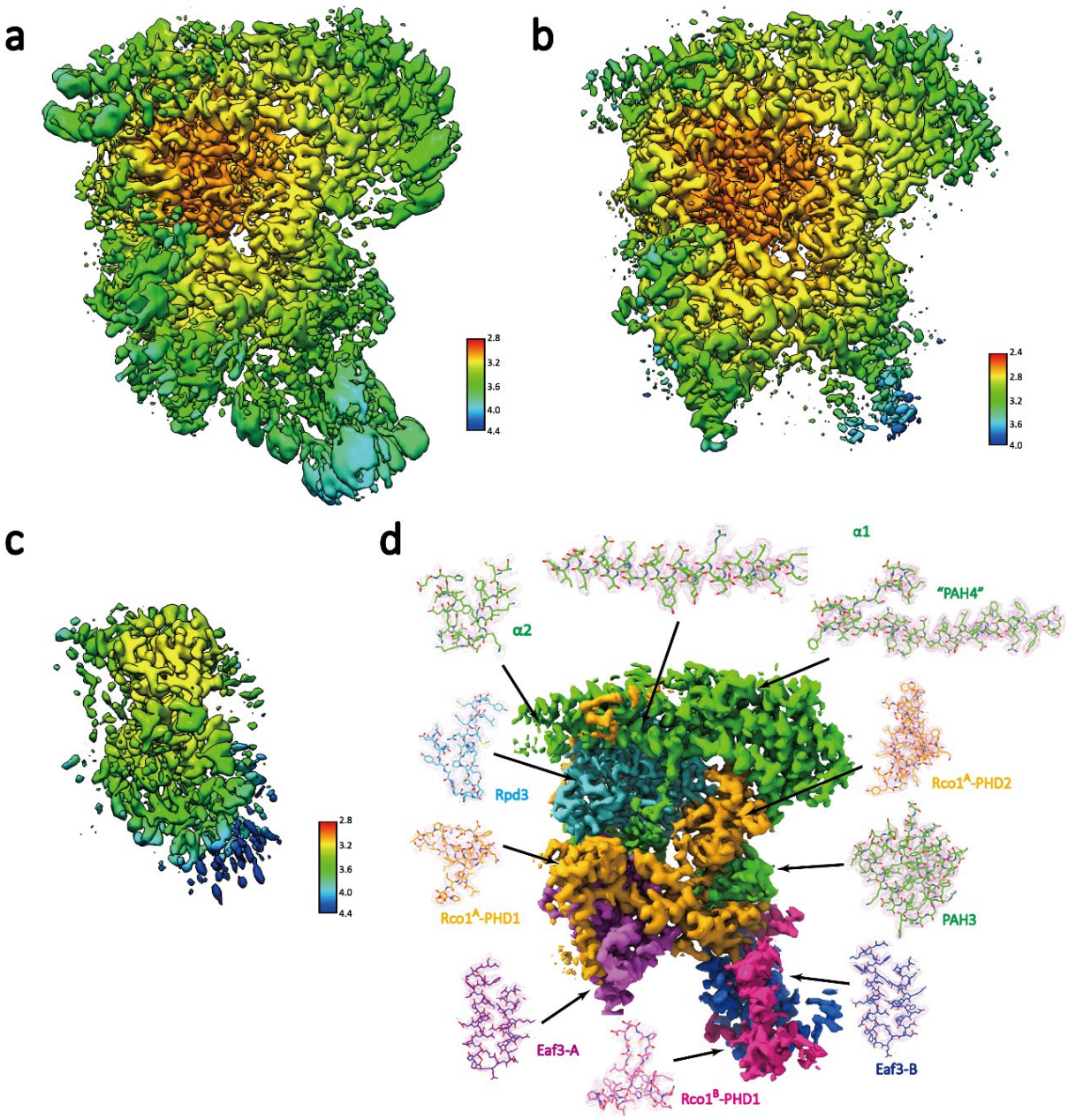

Extended Data Figure 4

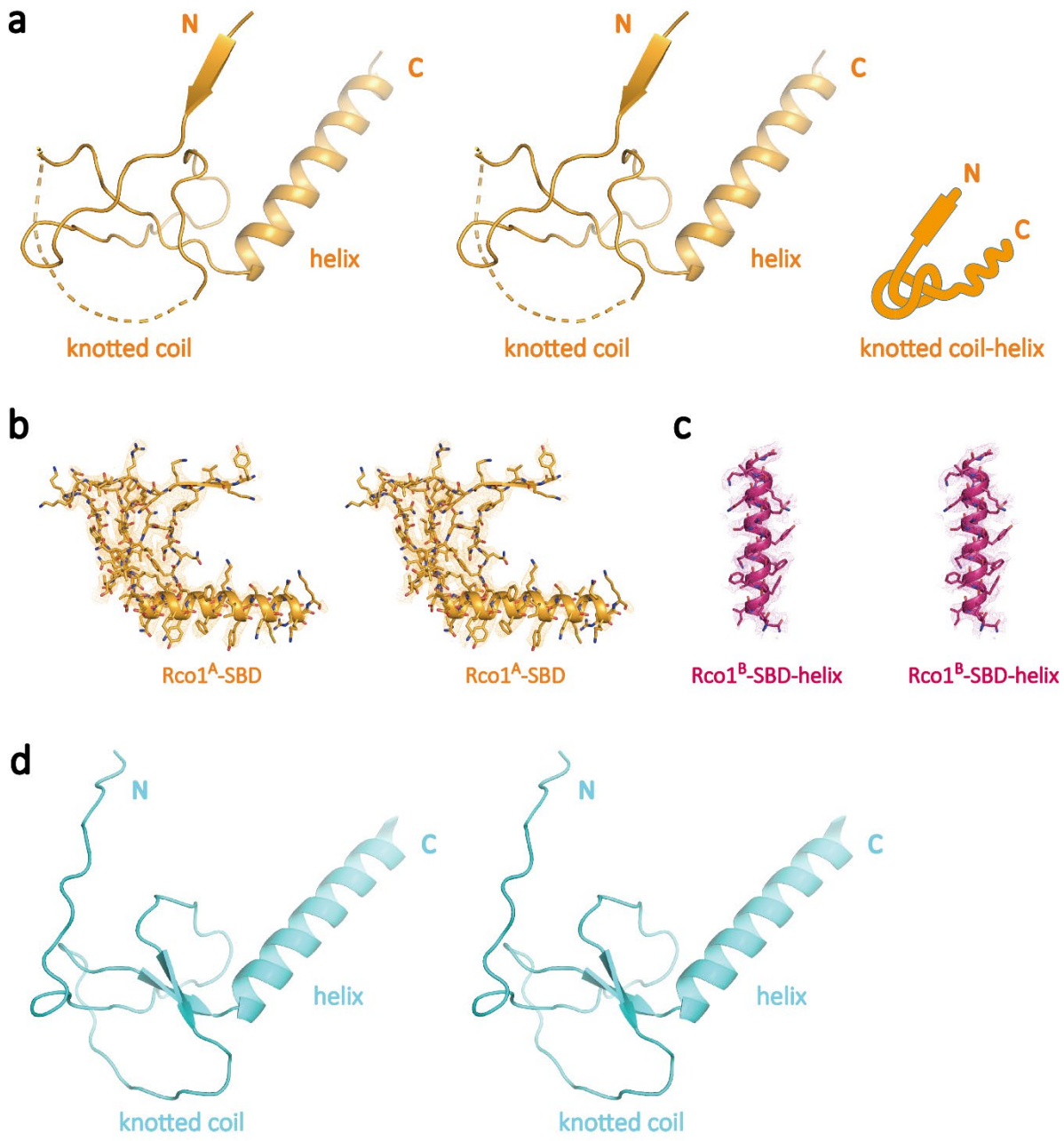

Extended Data Figure 5

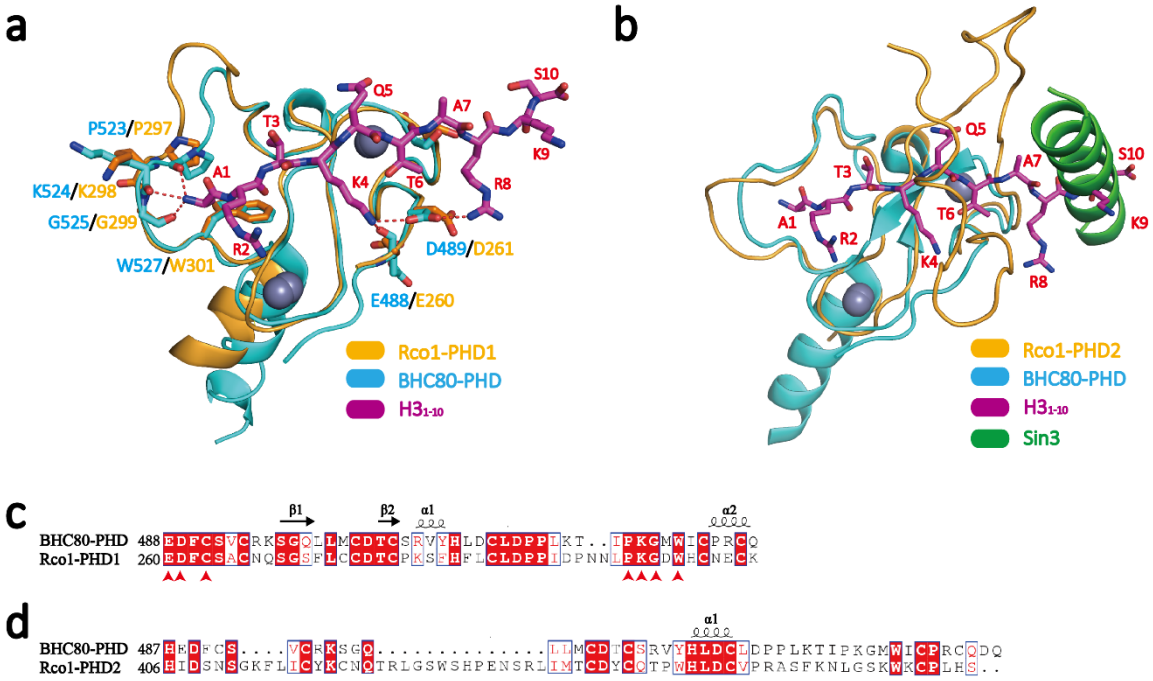

Extended Data Figure 6

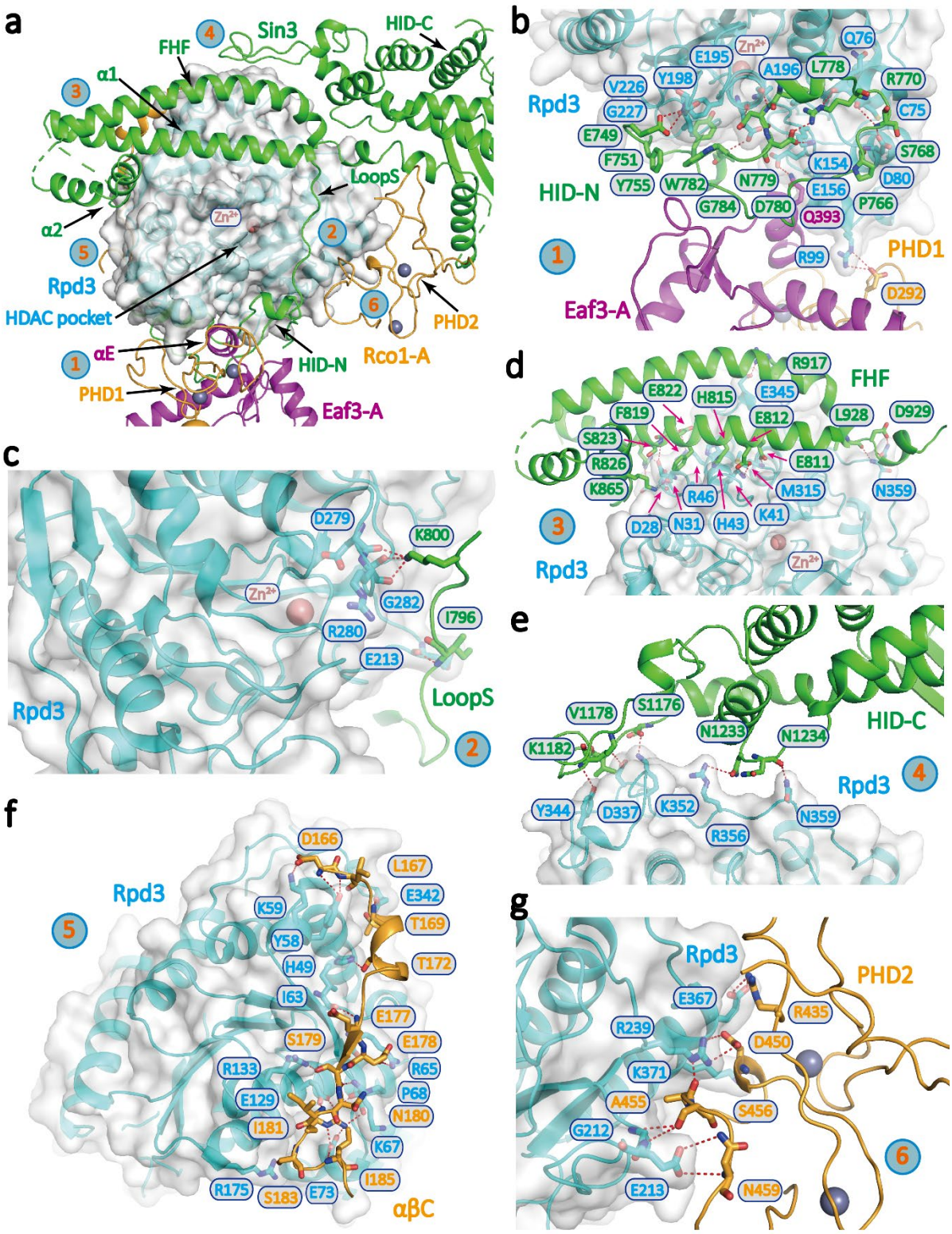

Extended Data Figure 7

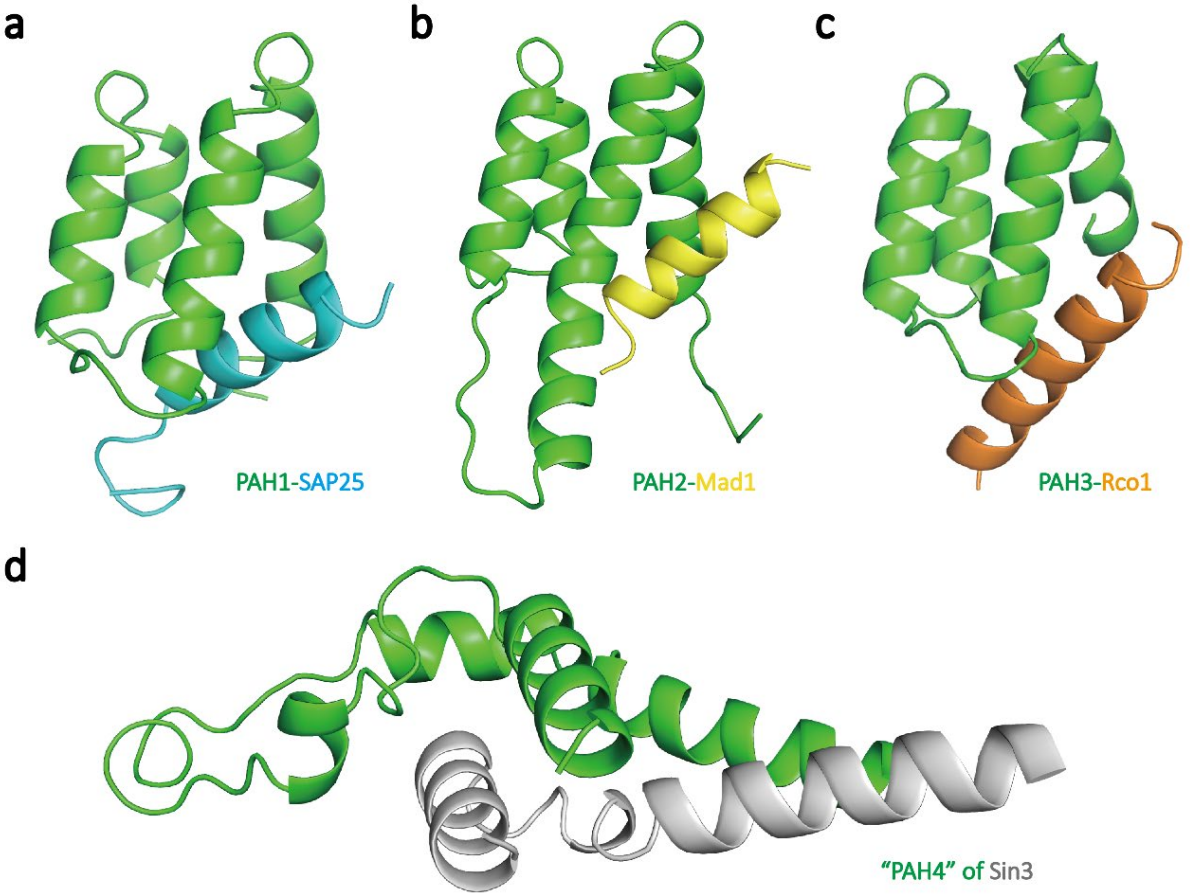

Extended Data Figure 8

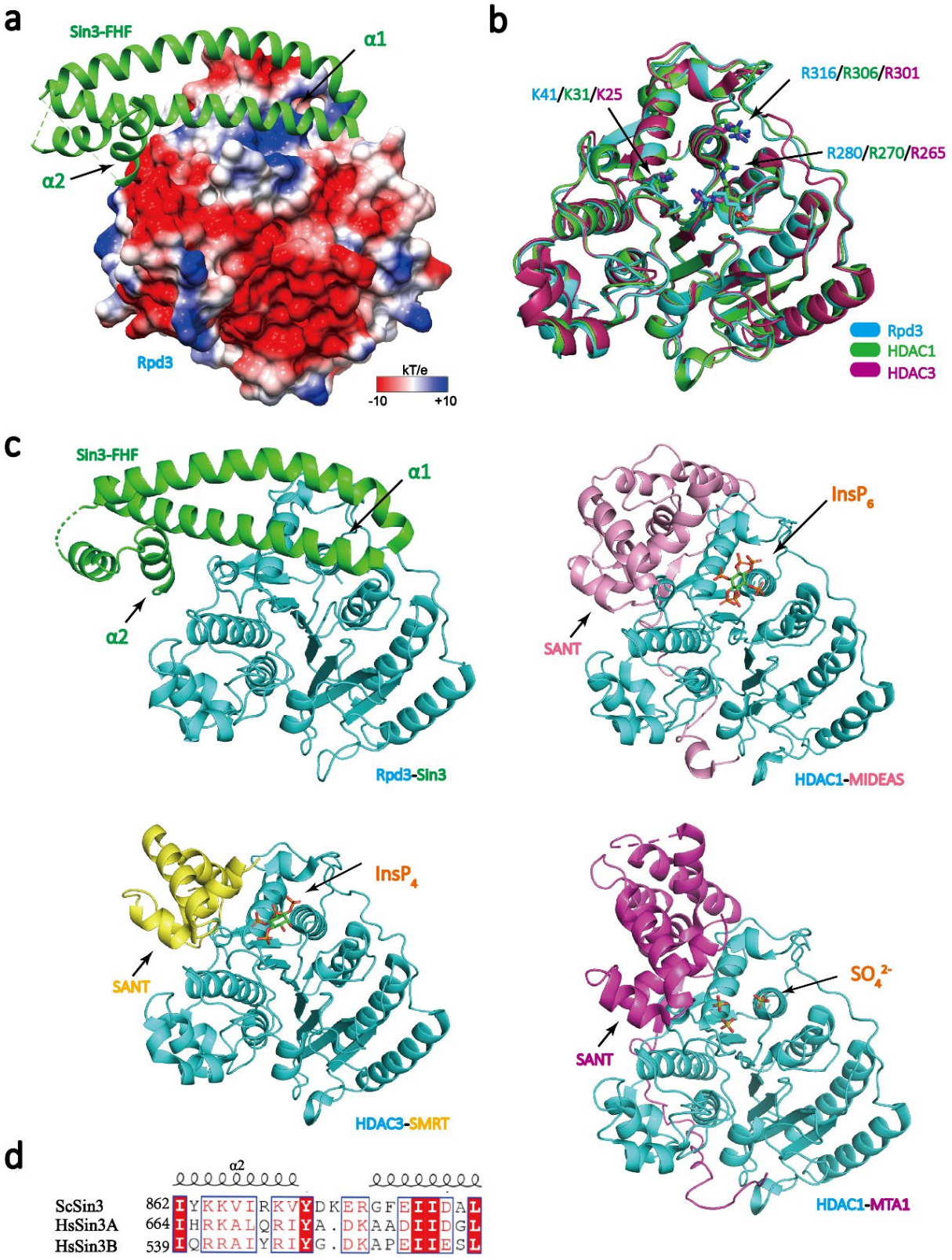

Extended Data Figure 9

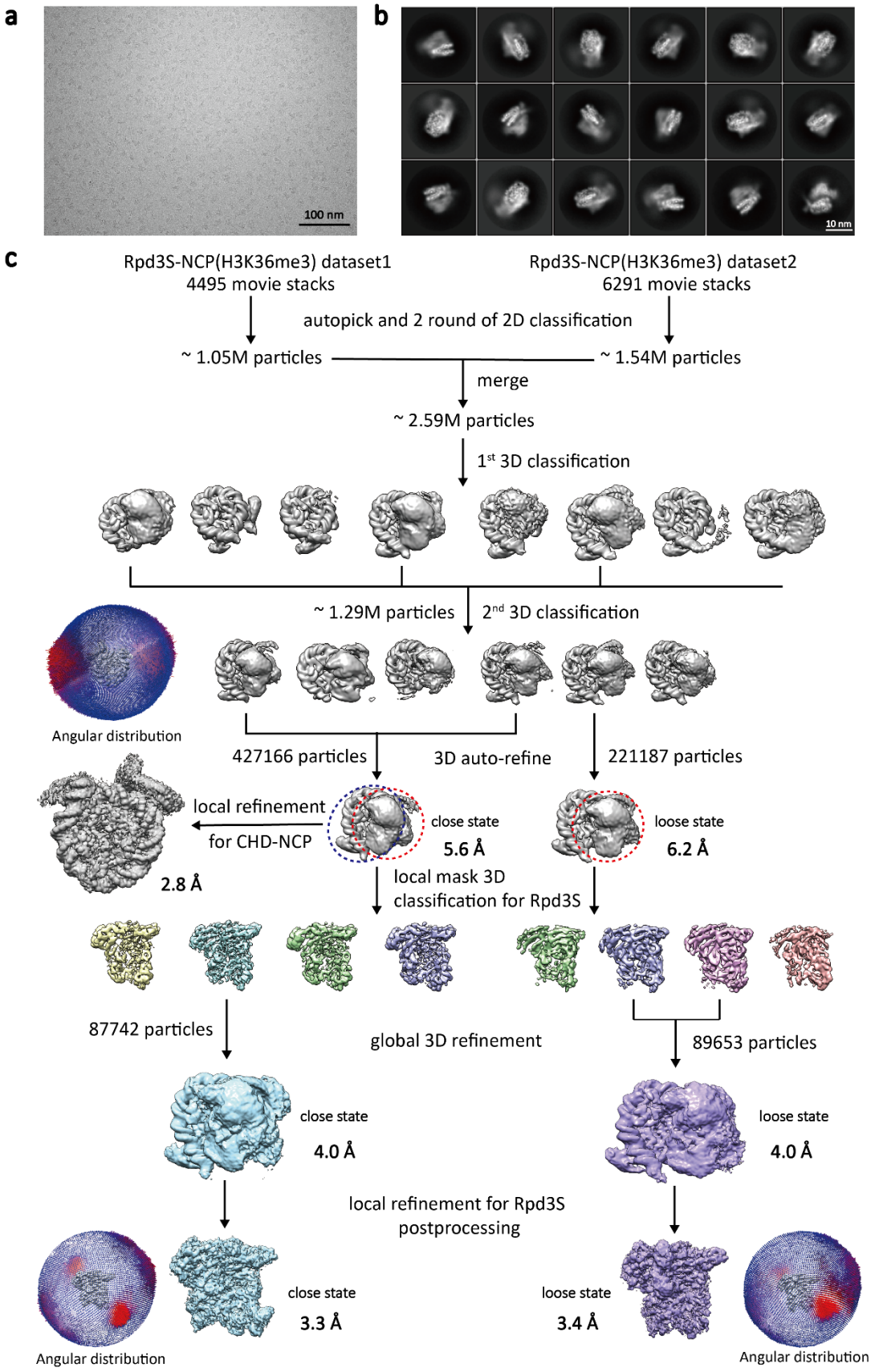

Extended Data Figure 10

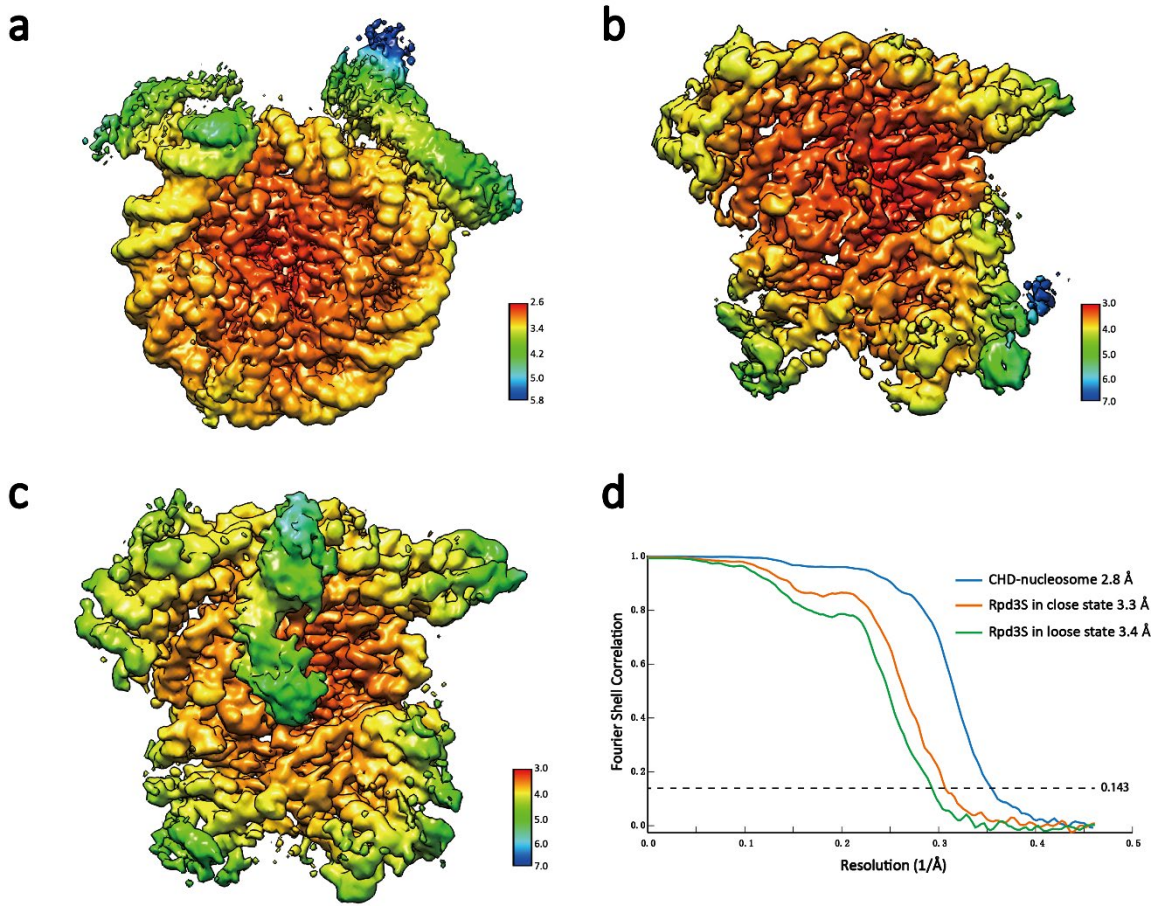

Extended Data Figure 11

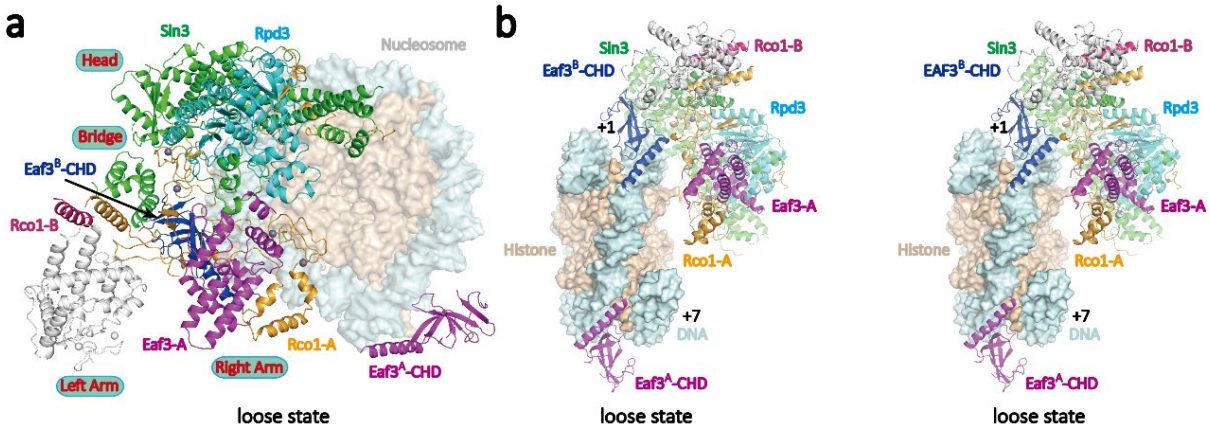

Extended Data Figure 12

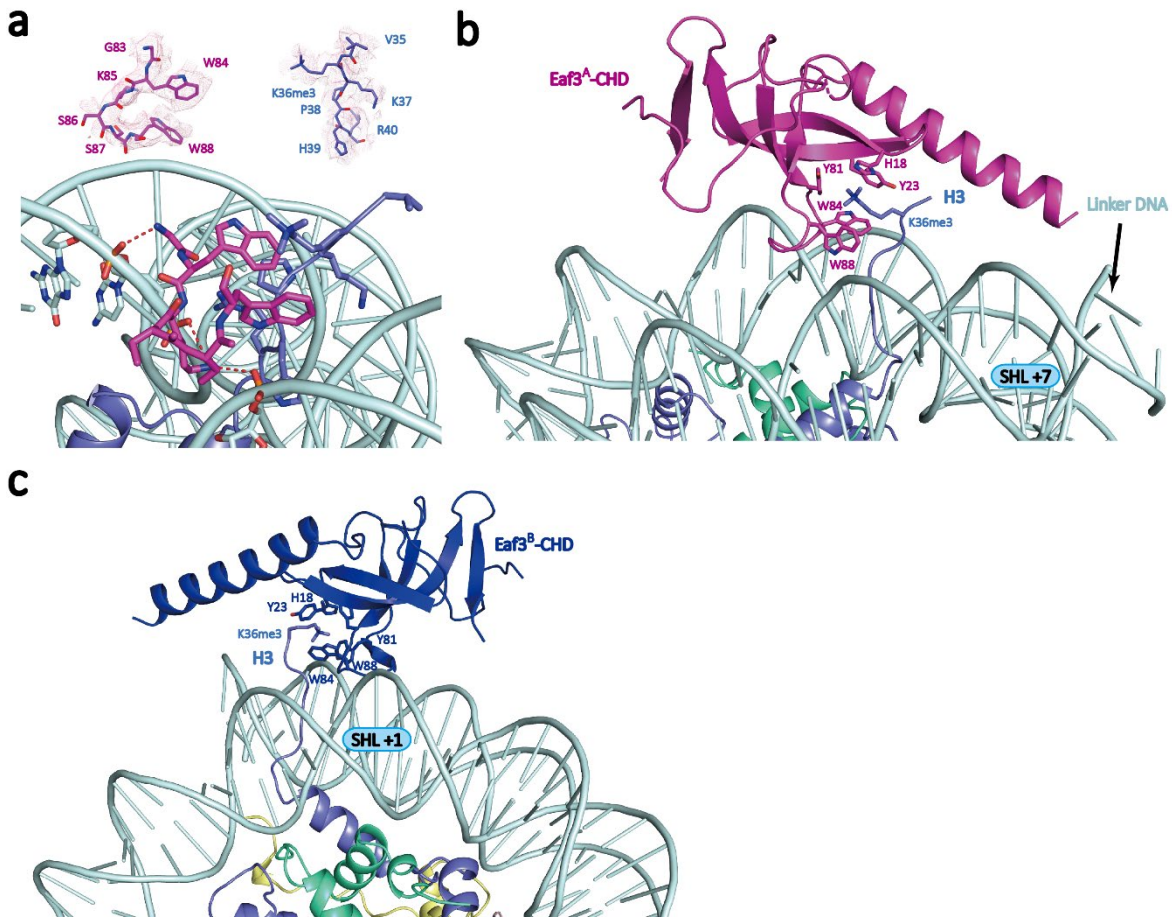

Extended Data Figure 13

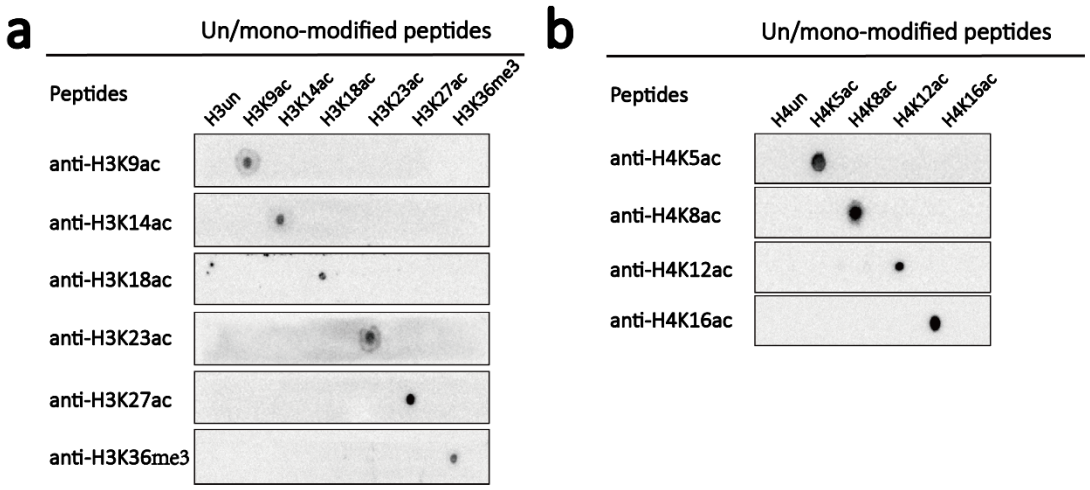

Extended Data Figure 14

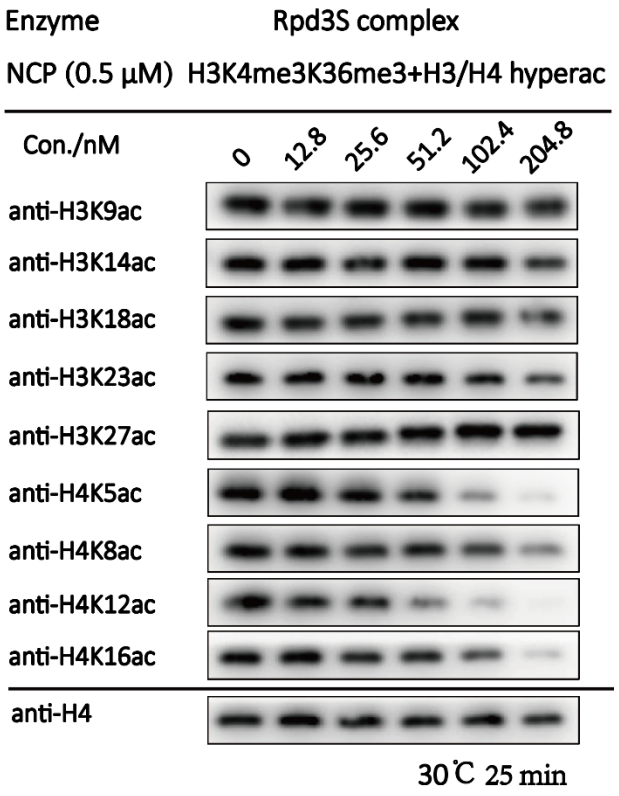

Extended Data Figure 15

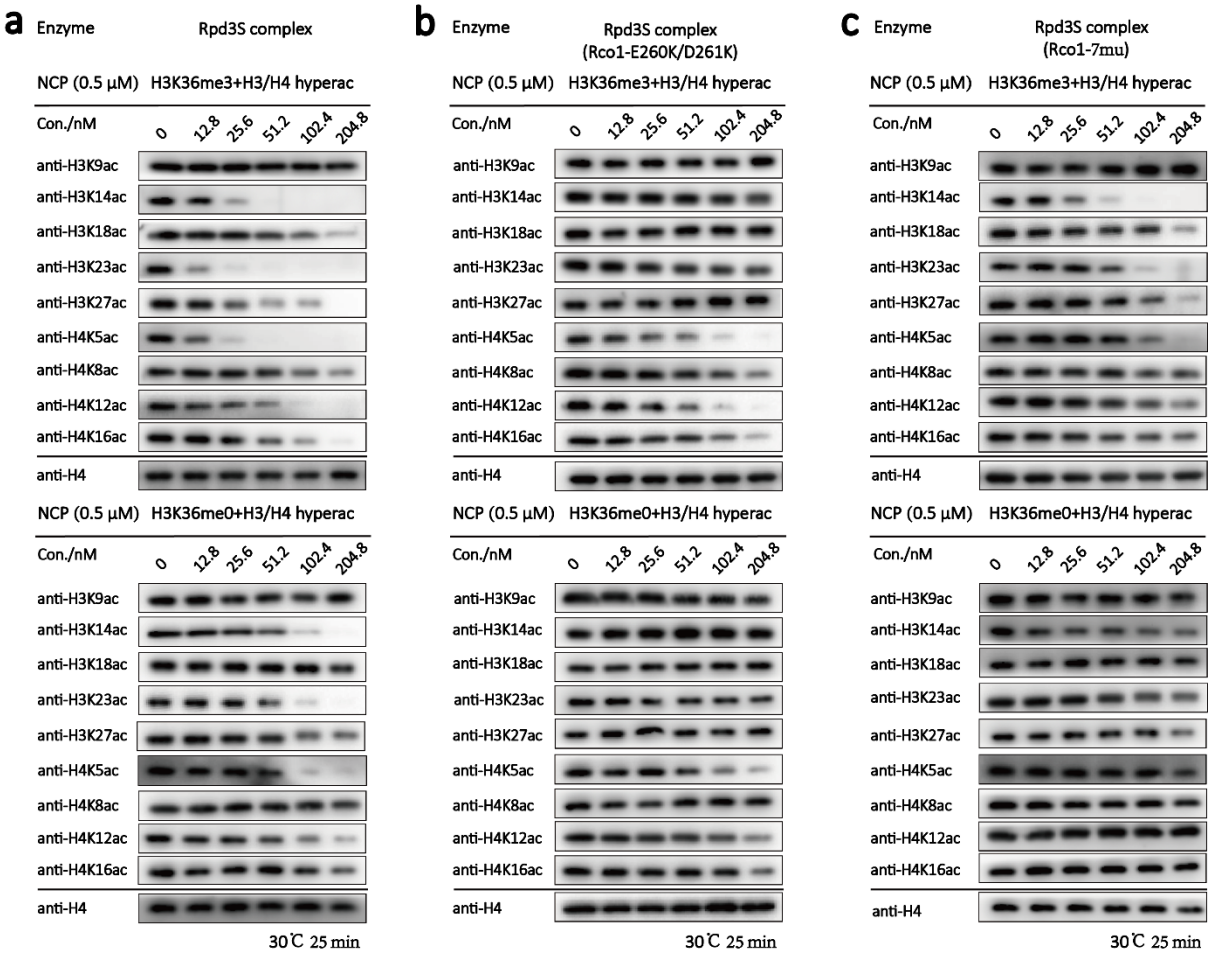

Extended Data Figure 16

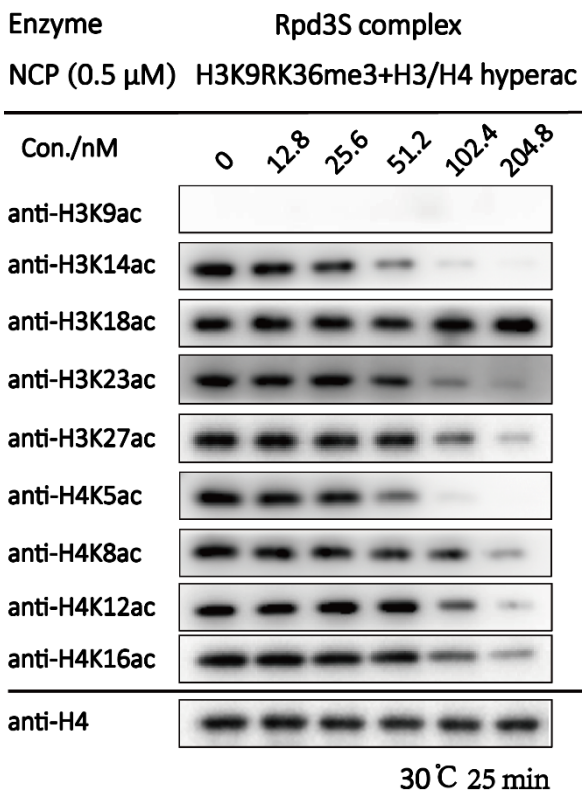

Extended Data Figure 17

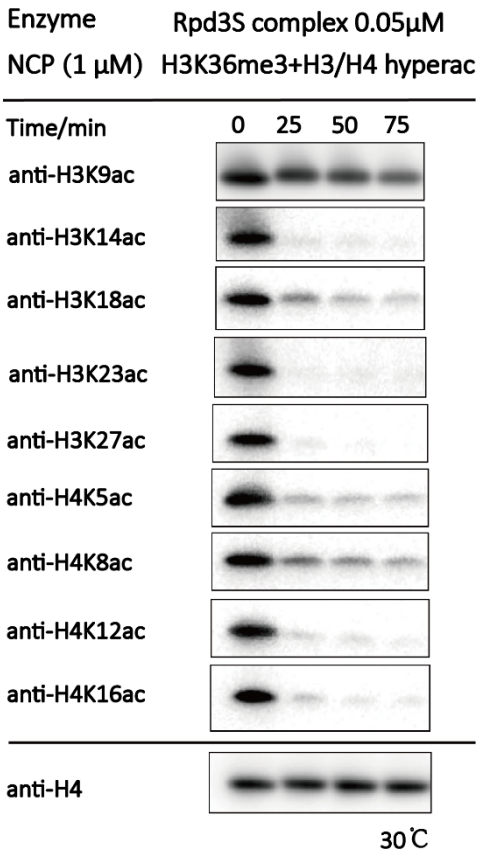

Extended Data Figure 18

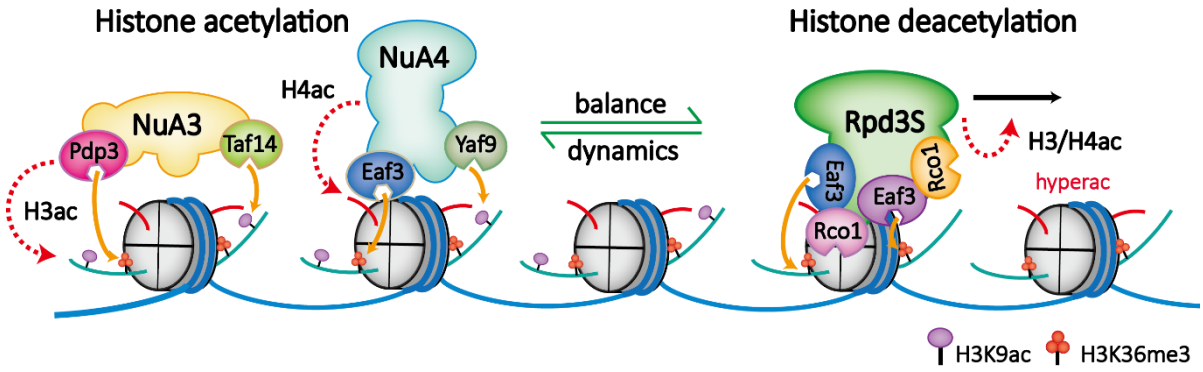

Extended Data Figure 19

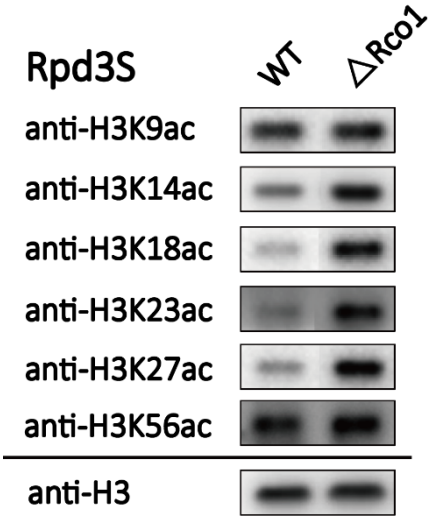

Extended Data Figure 20

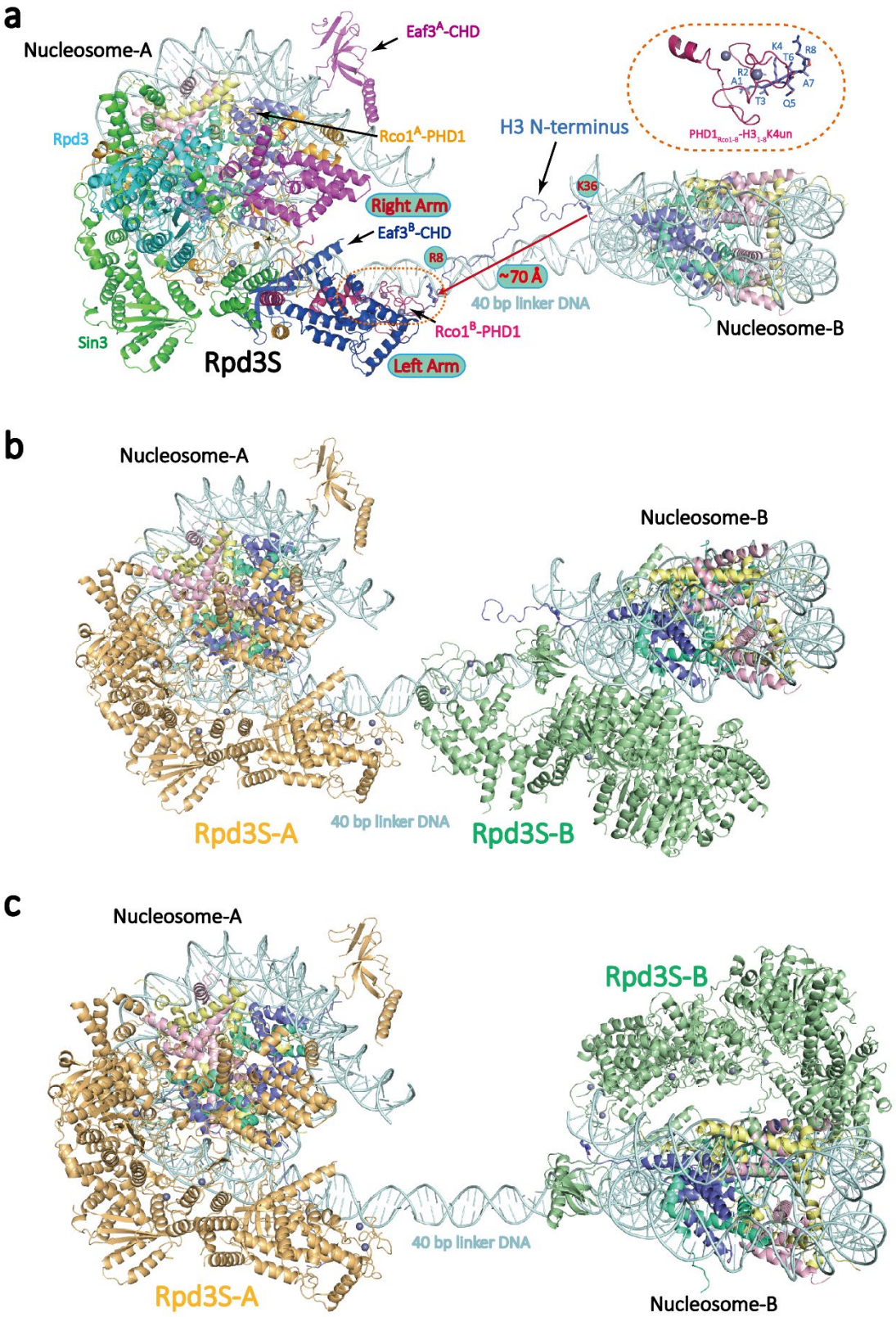

Supplementary Table 1. Cryo-EM data collection, refinement, and validation statistics of Rpd3S complex.

	Rpd3S complex	Rpd3S complex (head-bridge-right arm)	Rpd3S complex (left arm)
EMDB	33845	33846	33847
PDB	7YI0		
Data collection and processing			
Magnification	64000	64000	64000
Voltage (kV)	300	300	300
Electron exposure (e^-/ Å^2)	50	50	50
Number of frames per movie	32	32	32
Energy filter slit width (eV)	20	20	20
Automation software	AutoEMation2	AutoEMation2	AutoEMation2
Defocus range (μm)	-1.8 to -2.5	-1.8 to -2.5	-1.8 to -2.5
Pixel size (Å)	1.10	1.10	1.10
Symmetry imposed	C1	C1	C1
Micrographs (no.)	6990	6990	6990
Initial particles images (no.)	2.63 M	2.63 M	2.63 M
Final particles images (no.)	466 K	466 K	466 K
Map resolution (Å)	3.2	2.7	3.2
FSC threshold	0.143	0.143	0.143
Map resolution range (Å)	2.5-3.5	2.5-3.5	2.7-3.5
Map sharpening B-factor (Å^2)	-147.8	-70.9	-108.1
Refinement			
Refinement package	Phenix		
R.m.s. deviations			
Bond lengths (Å)	0.003		
Bond angles (°)	0.567		
Validation			
MolProbity score	1.84		
Clashscore	8.46		
Rotamer outliers (%)	0.93		
Cβ outliers (%)	0.00		
CaBLAM outliers (%)	3.31		
EMRinger score	3.23		
Overall correlation coefficients			
CC (mask)	0.80		
CC (box)	0.79		
CC (peaks)	0.75		
CC (volume)	0.81		
Ramachandran plot			
Favored (%)	94.33		
Allowed (%)	5.67		
Disallowed (%)	0.00		

Supplementary Table 2. Cryo-EM data collection, refinement, and validation statistics of Rpd3S-nucleosome.

	CHD-NCP	Rpd3S (close state)	Rpd3S (loose state)	Rpd3S-NCP (close state)	Rpd3S-NCP (loose state)
EMDB	33848	33850	33849	33851	33852
PDB	7YI1	7YI3	7YI2	7YI4	7YI5
Data collection and processing					
Magnification	64000	64000	64000	64000	64000
Voltage (kV)	300	300	300	300	300
Electron exposure (e^-/ Å^2)	50	50	50	50	50
Number of frames per movie	32	32	32	32	32
Energy filter slit width (eV)	20	20	20	20	20
Automation software	AutoEMatio n2	AutoEMatio n2	AutoEMatio n2	AutoEMatio n2	AutoEMatio n2
Defocus range (μm)	-1.8 to -2.5	-1.8 to -2.5	-1.8 to -2.5	-1.8 to -2.5	-1.8 to -2.5
Pixel size (Å)	1.08	1.08	1,08	1.08	1.08
Symmetry imposed	C1	C1	C1	C1	C1
Micrographs (no.)	10786	10786	10786	10786	10786
Initial particles images (no.)	2.59 M	2.59 M	2.59 M	2.59M	2.59M
Final particles images (no.)	427K	87.7K	89.6K	87.7 K	89.6 K
Map resolution (Å)	2.8	3.3	3.4	4.0	4.0
FSC threshold	0.143	0.143	0.143	0.143	0.143
Map resolution range (Å)	2.5-6.0	2.8-5.8	2.8-6.0	3.5-9.5	3.5-10.0
Map sharpening B-factor (Å^2)	-85.2	-85.0	-100.5	-113.143	-120.048
Refinement					
Refinement package	Phenix	Phenix	Phenix	Phenix	Phenix
R.m.s. deviations					
Bond lengths (Å)	0.003	0.003	0.003	0.004	0.005
Bond angles (°)	0.562	0.523	0.594	0.608	0.662
Validation					
MolProbity score	1.40	1.83	1.95	1.81	2.01
Clashscore	7.33	7.77	9.63	10.64	15.59
Rotamer outliers (%)	0.37	0.00	0.23	0.00	0.00
Cβ outliers (%)	0.00	0.00	0.00	0.00	0.00
CaBLAM outliers (%)	0.98	2.93	3.59	2.18	2.35
EMRinger score	2.94	2.60	2.10	0.23	0.30
Overall correlation					
CC (mask)	0.84	0.77	0.77	0.82	0.84
CC (box)	0.81	0.73	0.75	0.85	0.87
CC (peaks)	0.74	0.62	0.62	0.77	0.78
CC (volume)	0.82	0.75	0.75	0.82	0.84
Ramachandran plot					
Favored (%)	98.09	93.91	93.12	96.13	95.49
Allowed (%)	1.91	6.09	6.88	3.87	4.51
Disallowed (%)	0.00	0.00	0.00	0.00	0.00

Supplementary Table 3. Yeast Strains used in this study.

Strains	Genotypes	Source
W303-1a	*MATa, leu2-3, 112, ura3-1, his3-11,15, trp1-1, ade2-1, can1-100*	Q. Li
YBL534	*MATa,his3Δ1 leu2Δ0 met15Δ0 ura3Δ0* ***RCO1Δ::KANMX6***	B. Li
YBL853	*MATa, his3Δ1 leu2Δ0 met15Δ0 ura3Δ0* ***RCO1Δ::KANMX6 STE11-1870::HIS3***	B. Li